Long-Term Interaction of Submerged Tunnels with Rheological Rock Masses & Time-Dependent Permeability

Geotech Geol Eng (2025) 43:142
https://doi.org/10.1007/s10706-025-03103-4

ORIGINAL PAPER

Long-Term Interaction of Submerged Tunnels with Rheological Rock Masses & Time-Dependent Permeability

Milad Zaheri · Masoud Ranjbarnia · Pierpaolo Oreste

Received: 10 October 2024 / Accepted: 24 February 2025

Abstract Submerged tunnels may pass through rock types and may encounter a variety of difficult geological conditions. One of these challenging conditions is confronting with highly stressed weak rock masses. The challenge pertaining to design of these tunnels is intensified when water seepage occurs into tunnel. In this condition, the rheological behavior of the rock mass causes the pressure acting on the lining to enhance over time, and consequently, the permeability coefficient of the rock mass in any point is changed over time. This paper investigates this problem, the tunnel construction process is all simulated in this study. Furthermore, based on the rock mass volumetric strain, a time-dependent variable permeability is assigned to the rock mass around the tunnel. A parametric study is conducted to evaluate the effect of rock mass rheological parameters, the internal water pressure, and the ratio of the rock mass and lining permeability on the submerged tunnel behavior. The results show that the internal water pressure extremely influences the tunnel response. Moreover, the permeability variation of the rock mass should be necessary, but unfortunately this is not feasible in most computer codes for three-dimensional numerical modeling.

Keywords Submerged tunnels · Long-term behavior · Weak rock mass · Time-dependent permeability · Tridimensional numerical modelling

1 Introduction

Most of rock engineering projects involve sedimentary rock masses, which are classified as soft rock masses, such as schist, shale, and sandstone (Kanji et al 2019; Li et al. 2023; Zaheri et al. 2023a; Pelizza et al. 2000; de Rienzo et al. 2009). These soft rock masses when located at great depths show extreme squeezing and a time-dependent behavior. Therefore, e.g., in tunnels, the induced pressure on the lining increases over time; sometimes the phenomenon can be dangerous because it can lead to breakage.

The issue of the time-dependent behavior of tunnels in soft rocks has been comprehensively investigated, and numerous numerical and analytical studies have been conducted. In these cases, it is not possible to adopt simplified approaches such as those

M. Zaheri · M. Ranjbarnia
Department of Geotechnical Engineering, Faculty of Civil Engineering, University of Tabriz, Tabriz, Iran
e-mail: Miladzaheri@tabrizu.ac.ir

M. Ranjbarnia
e-mail: M.ranjbarnia@tabrizu.ac.ir

M. Ranjbarnia
Institute of Geoscience, Christian-Albrecht's-University of Kiel, Kiel, Germany

P. Oreste (✉)
Department of Environmental, Land and Infrastructure Engineering, Politecnico di Torino, Turin, Italy
e-mail: pierpaolo.oreste@polito.it

Published online: 25 March 2025

developed for other areas of tunnel stability study (Ranjbarnia et al. 2014; Oreste 2009; Do et al. 2015). These studies have followed up different aspects of the time-dependent behavior such as:

- installation time of the tunnel lining and its response over time (e.g., Nomikos et al. 2011; Wang et al. 2013; Kargar 2019; Wu and Shao 2019a, 2019b; Wu et al. 2019, 2020a, b, c, d; Chu et al. 2019, 2020, 2021; Do et al. 2020, 2021; Zhou et al. 2021; Guo et al. 2021; Zhao et al. 2022; Hongming et al. 2024; Lu et al. 2024);
- tunnel excavation speed (e.g.,Paraskevopoulou and Diederichs 2018; Chu et al. 2019, 2020);
- different rheological behavior of rock masses (e.g., Fahimifar et al. 2010; Tran Manh et al. 2015; Zhang et al. 2020; Song et al. 2022; Tarifard et al. 2022; Hu and Gutierrez 2023; Jing et al. 2023; Liu et al. 2023; Zaheri et al. 2024a, b, 2025; Zeng et al. 2024; Chen et al. 2025; Liang et al. 2025; Ai et al. 2025);

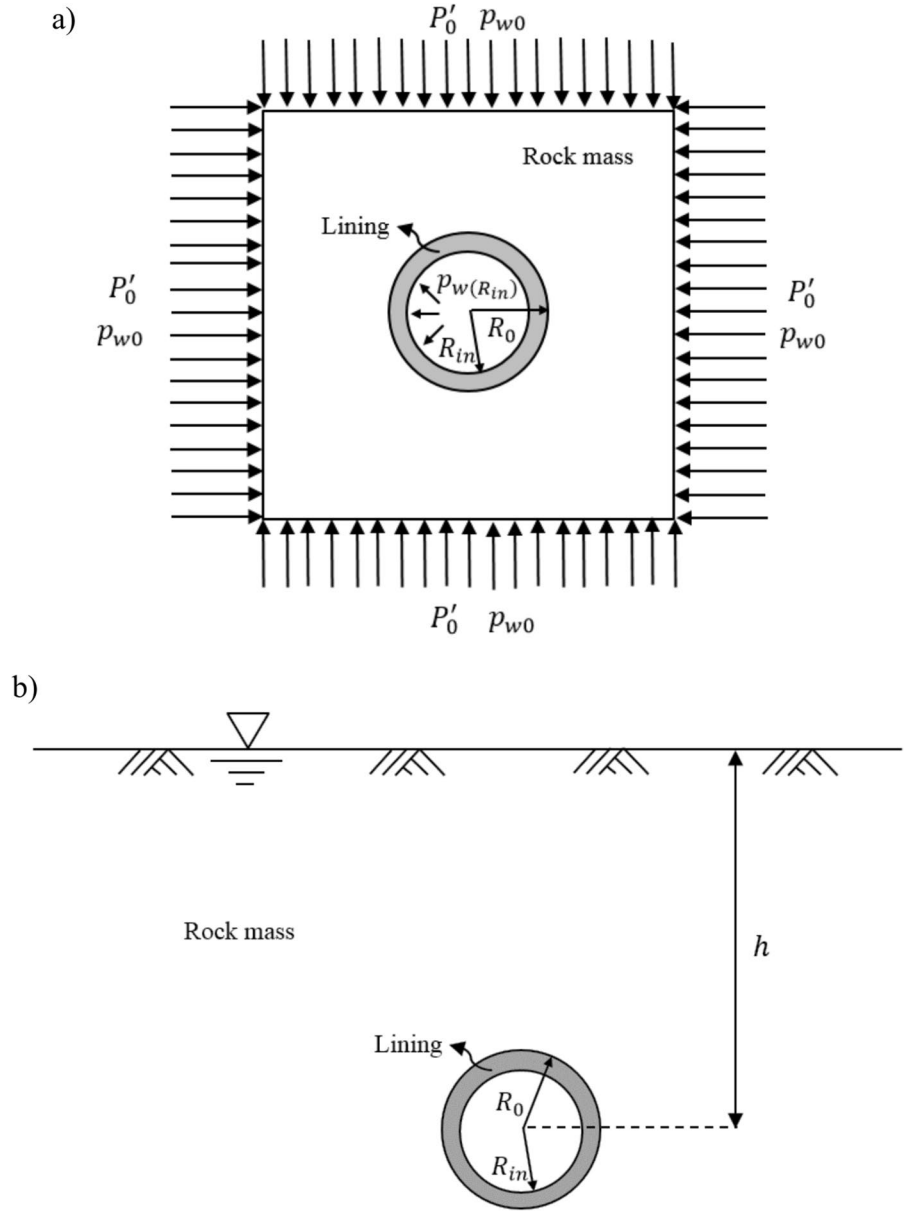

Fig. 1 The geometry of the model. Key: P_0': initial in-situ effective stress,p_{w0}: initial pore water pressure,$p_{w(R_{in})}$: pore water pressure at the inner radius of the lining,R_0: outer radius of the lining,R_{in}: inner radius of the lining

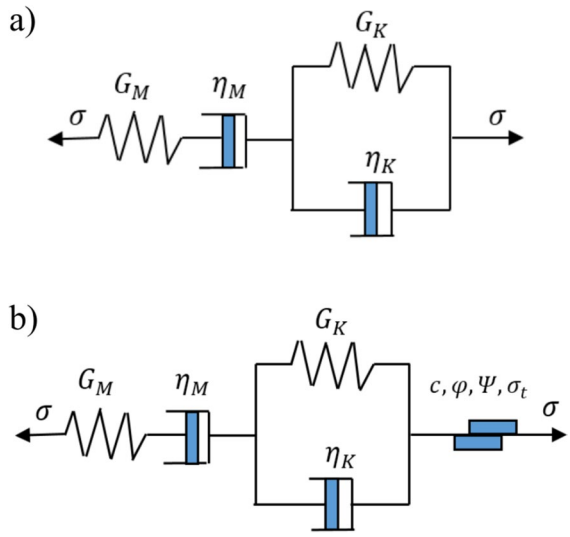

Fig. 2 **a** Burgers model, **b** CVISC model. Key: σ: stress, G_M: Maxwell shear modulus, G_K: Kelvin shear modulus,η_M: Maxwell viscosity, η_K: Kelvin viscosity, c: cohesion, φ: friction angle, Ψ: dilation angle, σ_t: tension strength

- effects of in-situ stresses (e.g.,Kargar and Haghgouei 2020; Kargar et al. 2020; Wang et al. 2020, 2023);
- effects of the tunnel shape (Wang et al. 2019; Zeng et al. 2020); and
- considering the excavation damaged zone around tunnels (Zaheri et al. 2022; Zaheri and Ranjbarnia 2021, 2023a, b; 2024) and etc.

One of the major challenges in submerged tunnels is the interaction between the tunnel lining and the surrounding rock mass, particularly considering the seepage of water. This seepage can occur from the tunnel lining into the surrounding rock mass, or vice versa. This phenomenon leads to additional stresses on the tunnel lining. The development of pore water pressure as well as seepage of water in the surrounding rock mass, is influenced by various factors, including the phases of tunnel construction. These phases include the tunnel excavation, installation of a lining, and the filling of the tunnel with water to transport water from a reservoir to a powerhouse.

Bobet (2001) analyzed the behavior of shallow tunnels with and without drainage at the ground-lining interface, assuming for both soil and lining an elastic behavior. Bobet and Nam (2007) proposed a solution to find out the role of seepage and slope angle on the tunnel behavior, when the tunnel is constructed on a slope. Brown and Bray (1982) investigated the influence of permeability in the plastic zone around the tunnel on the performance of deep circular tunnels. Bobet (2010) clarified the influence of seepage force on the response of deep tunnels embedded in rock masses. Carranza-Torres and Zhao (2009) evaluated the drainage condition of the lining and its effect on the induced pressure. Dadashi et al. (2017) considered the coupled hydro-mechanical interaction (simultaneous effects of water seepage and rock mass properties to each other) in the analysis, and simulated the effect of lining cracks due to the high internal water pressure. Zareifard and Fahimifar (2016b) and Zareifard and Shekari (2021) investigated the effect of poor-blasting damage of rock masses on the response of deep submerged tunnels tunnels. The issue of different seepage patterns of water inflation into a tunnel, which can be due to the rock mass permeability value, was studied by Fahimifar et al., (2014), (2015a, b); Fahimifar and Zareifard (2014); Zareifard and Fahimifar (2016a).

It seems that most of the studies for the submerged tunnels is pertaining to non-squeezing conditions, which are not applicable for time-dependent behavior. Due to the fact that the rock mass with a rheological behavior causes the pressure acting on the lining to enhance over time, the stress field around the tunnel is altered; moreover, the permeability coefficient in each point of the rock mass changes over time. It may lead the stress induced by the water seepage to the lining to vary.

Therefore, a need arises to cover the above-mentioned gap in order to study the simultaneous influence of the water seepage and the time-dependent behavior of the rock mass on each other. Indeed, as discussed above, rock mass deforms due to squeezing behavior, leading its permeability to change over time. This paper follows up this issue by using the numerical simulation with FLAC^{3D}. However, like most numerical software, as this program takes a unique permeability coefficient that is not altered during the analysis, a specific numerical procedure is developed in order to consider the permeability coefficient variability around the tunnel (this variability has been implemented in the software). The final aim is to investigate if this variability has a great influence or not, for future revision in software.

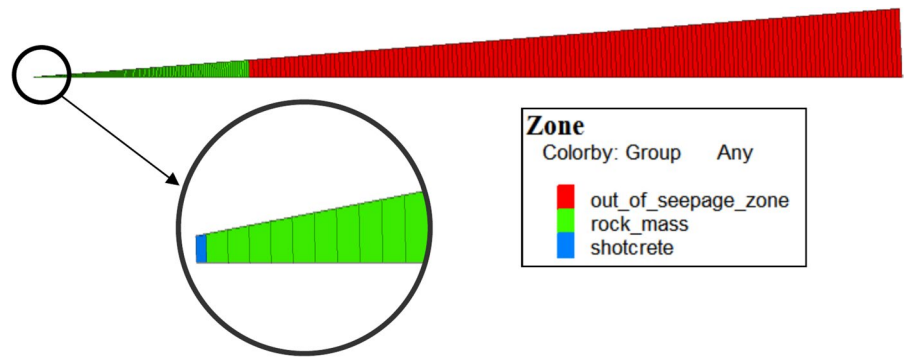

Fig. 3 Constructed model in FLAC^{3D} software

a)

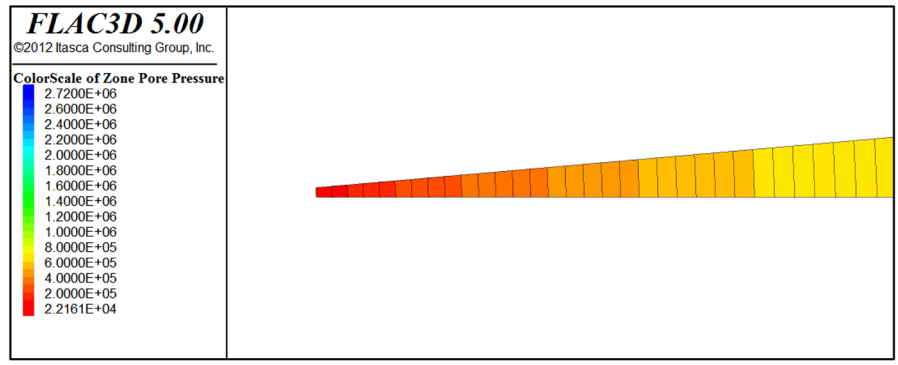

b)

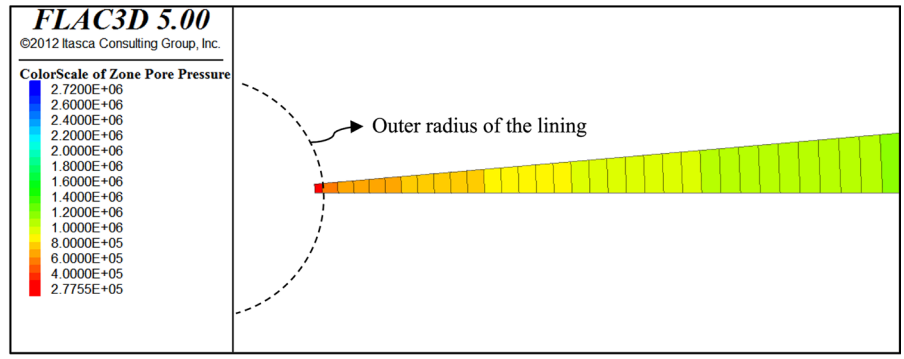

c)

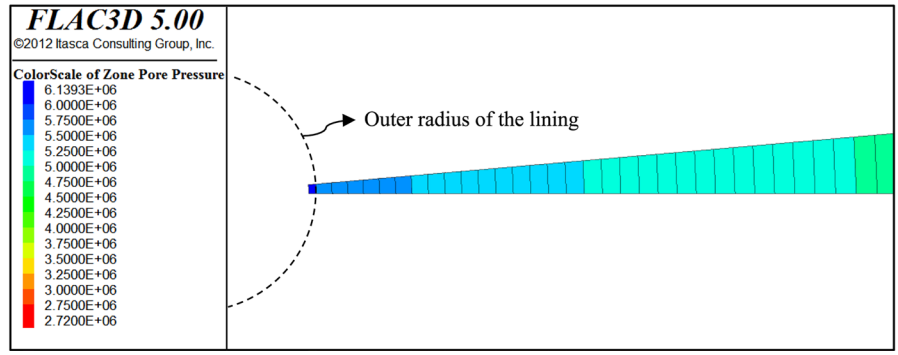

Fig. 4 Pore water distribution **a** before lining installation, **b** after lining installation, **c** after applying the internal water pressure (Unit: Pa)

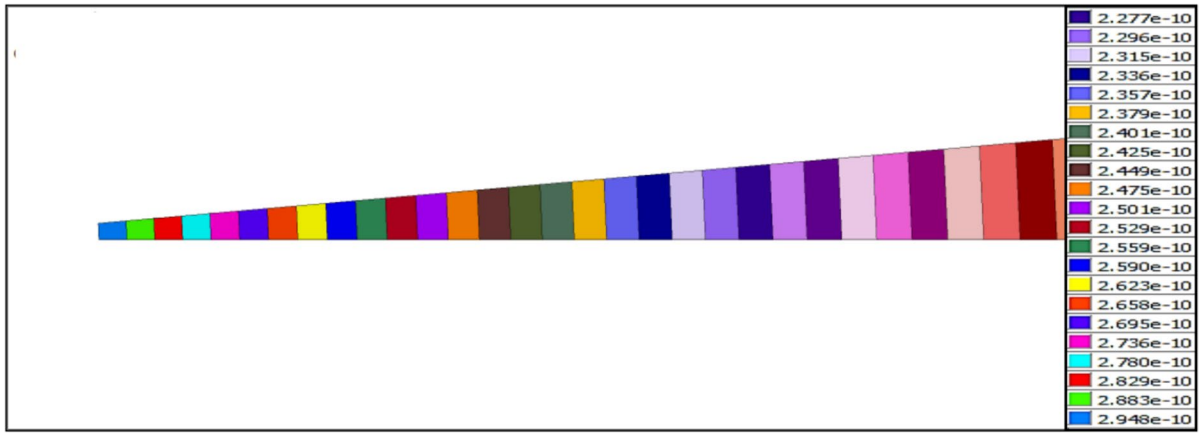

Fig. 5 Rock mass permeability coefficients in different zones $\left(\text{unit} : \frac{\text{m}}{\text{s}}\right)$

2 Problem Definition

A long tunnel with a circular cross-section with radius R_0 (See Fig. 1) is excavated in a saturated rock mass with rheological behavior. The initial in-situ effective stress is hydrostatic and equals to P_0' whereas the initial pore water pressure is p_{w0}.

The time-dependent behavior of the rock mass is described by the Burgers model or the CVISC model (i.e., Burgers-Mohr-Coulomb model), as observed in Fig. 2. The Burgers model consists of two shear

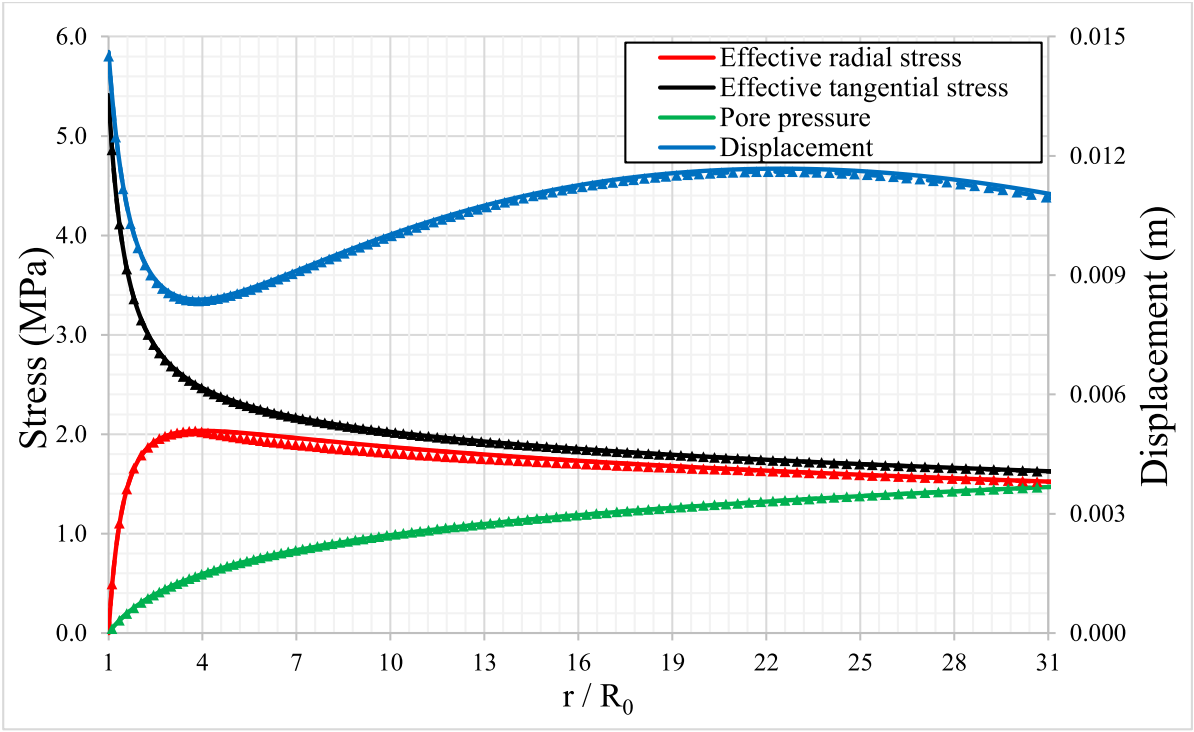

Fig. 6 Distributions of effective radial and tangential stresses, pore water pressure, and radial displacement varying the scaled distance from the center of the tunnel (the continuous lines and the triangle markers represent the results of the Bobet (2010) and FLAC^{3D} software, respectively). Key: r: radial distance from the tunnel center, R_0: tunnel radius

Table 1 Input data (Bobet 2010)

Parameter	Symbol	Unit	Value
Tunnel radius	R_0	m	3
Seepage radius of influence	r_{sep}	m	100
Initial total stress	P_0	MPa	3
Initial pore water pressure	p_{w0}	MPa	1.5
Pore water pressure at the tunnel boundary	$p_{w(R_0)}$	MPa	0
Shear modulus of the rock mass	G_M	MPa	315
Poisson's ratio of the rock mass	v	–	0.35

moduli (G_M, G_K) and two viscosities (η_M, η_K), where subscripts M and K indicate the Maxwell and Kelvin models, respectively. In the CVISC model, if the applied stress does not meet the failure criterion, the model will be the Burgers model (Itasca Consulting Group, 2020).

The construction phases of the tunnel are idealized in three stages including:

(1) Tunnel excavation (before lining installation);
(2) Lining installation at time t_1; and
(3) Filling the tunnel with water at time t_2 to transport water from a reservoir to a powerhouse.

3 Numerical Simulation by the Tridimensional Numerical Modelling

The adopted running procedures consist of the following steps:

- *The preliminary simulation*
  - *Setting up the model:* Due to the axisymmetric conditions, only a sector of the model is considered. The length of the model along the radial direction is considered as 8 times of the tunnel depth to avoid unpredicted effects of the boundary location on the results. Note that the displacement behavior for dry and saturated rock masses exhibits notable differences. For the dry rock mass, displacement decreases with increasing distance from the tunnel boundary. However, when the effect of water flow is

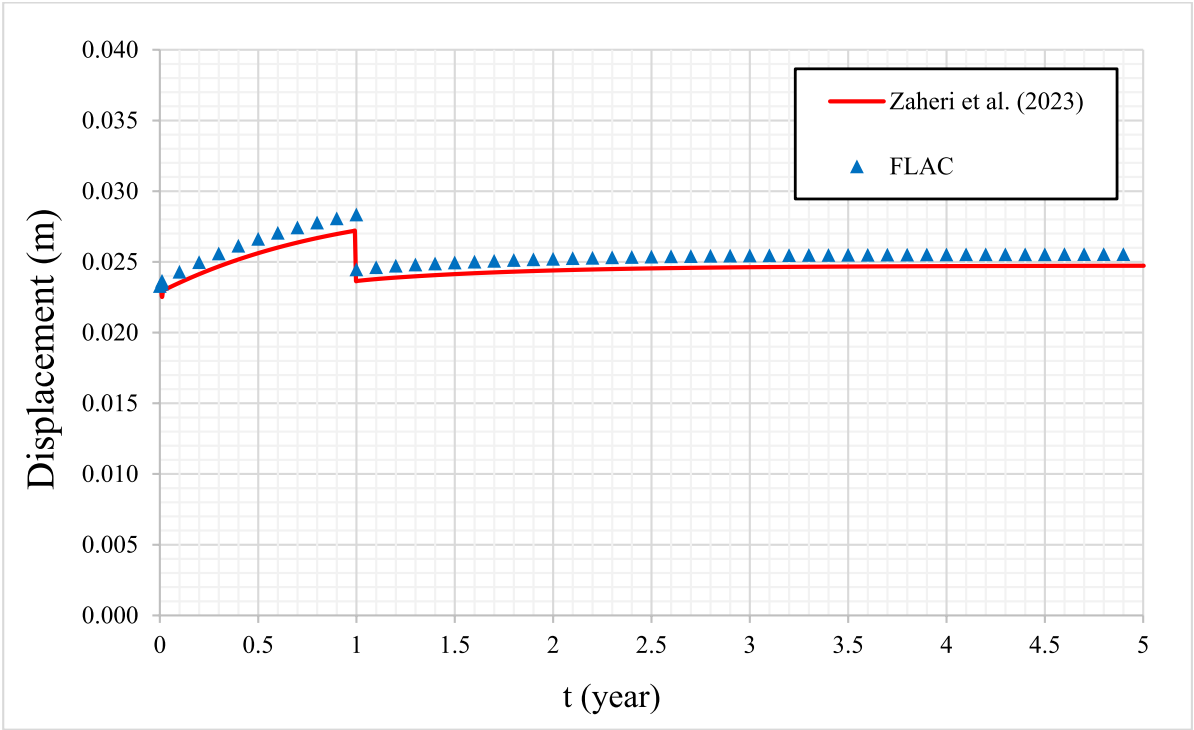

Fig. 7 Distribution of tunnel wall displacement over time (t)

included, a more complex displacement pattern emerges (See for example Fig. 6). Initially, the displacement decreases with distance from the tunnel, but at greater distances, it increases before ultimately decreasing again. Thus, when the external boundary of the model is chosen to be smaller, greater displacements will be occurred at the boundaries. This results indicate that the location of the model boundary can significantly influence the results. For this purpose, the length of the model is chosen eight times of the tunnel depth. Also, thanks to the assumed plain strain condition, the length of the model along the tunnel axis is considered 1 m. The seepage radius of influence is considered as $h+\sqrt{h^2-R_0^2}$ in which h is the distance between the tunnel center and the groundwater free surface (h parameter is shown in Fig. 1) (Kolymbas and Wagner 2007); Note that 2 different zones exist in this condition; The first zone has inner and outer radii equal to R_0 and $h+\sqrt{h^2-R_0^2}$. In this zone, water can seep towards the rock mass or vice versa. The other zone has inner and outer radii equal to $h+\sqrt{h^2-R_0^2}$ and 8 times of the tunnel depth, respectively. In this zone, pore water pressure is assumed to be constant, so the seepage force becomes zero (See Fig. 3).

- • *Applying the boundary conditions:* After assigning the in-situ total stress and pore water pressure to the model, these parameters are also applied to the right and left boundaries as shown in Fig. 3. The displacements are restricted such that only radial displacements can occur, due to the axisymmetric geometry;
- • *Assigning constitutive models*: The CVISC model or the Burgers model is assigned to the rock mass. As water seeps radially toward the tunnel and the permeability coefficients do not vary in the tangential direction, the isotropic flow model is assigned to the rock mass;
- *Running the initial condition*: This step is for checking the initial equilibrium state. Then, the nodal displacements and velocities are set to zero;

Table 2 Input data (Zaheri et al. 2023a, b)

Parameter	Symbol	Unit	Value
Inner radius of the lining	R_{in}	m	4.18
Outer radius of the lining	R_0	m	4.5
Initial effective stress	$P_0{}'$	MPa	4.08
Initial pore water pressure	p_{w0}	MPa	2.72
Pore water pressure at the inner radius of the lining after applying the internal water pressure	$p_{w(R_{in})}$	MPa	3.264
Lining installation time	t_1	day	4
Time of applying the internal water pressure (as a submerged tunnel)	t_2	day	365
Permeability of the rock mass	k_{ini}	m/s	10^{-6}
Permeability of the lining	k_{con}	m/s	10^{-7}
Maxwell shear modulus of the rock mass	G_M	MPa	658
Maxwell viscosity of the rock mass	η_M	MPa. year	132,500
Kelvin shear modulus of the rock mass	G_K	MPa	345
Kelvin viscosity of the rock mass	η_K	MPa. year	665
Friction angle of the rock mass	φ	°	33.95*
Cohesion of the rock mass	c	MPa	0.39*
Poisson's ratio of the rock mass	v	–	0.25
Shear modulus of the lining	G_{con}	MPa	13,125
Bulk modulus of the lining	K_{con}	MPa	17,500

*Calculated by RocLab software (Rocscience 2007)

a)

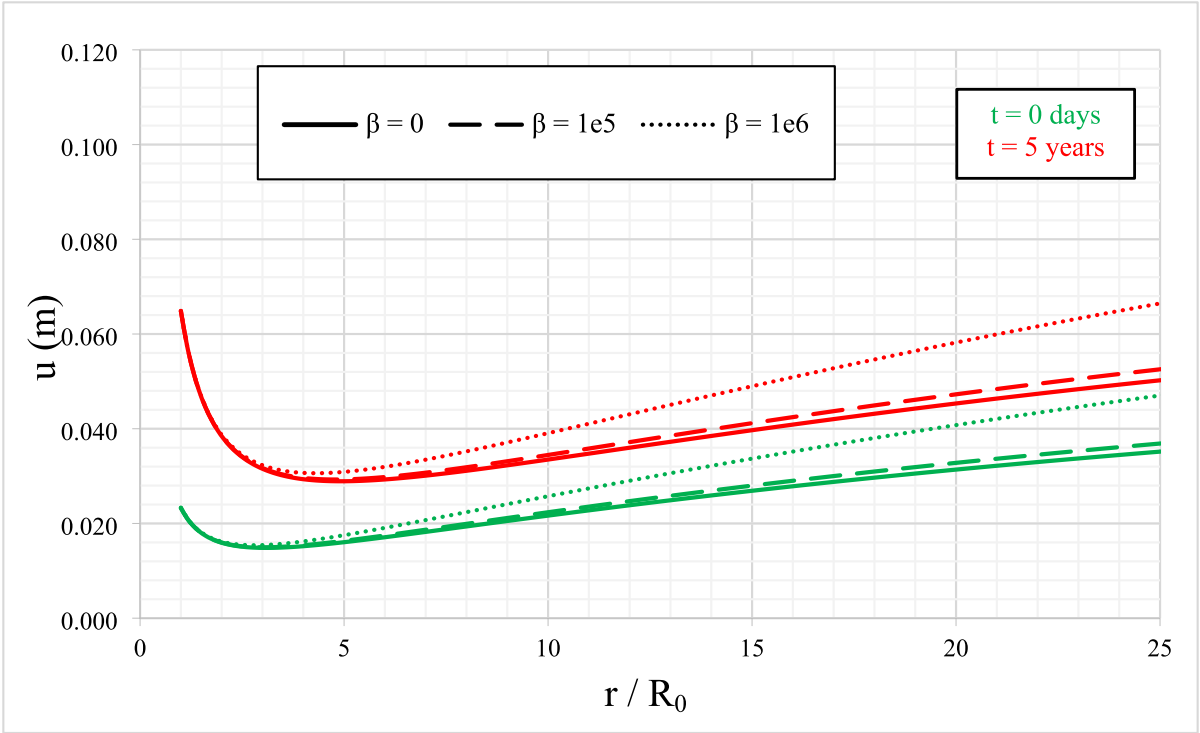
β = 0
β = 1e5
β = 1e6
t = 0 days
t = 5 years
u (m)
0.120
0.100
0.080
0.060
0.040
0.020
0.000
0
5
10
15
20
25
r / R0

b)

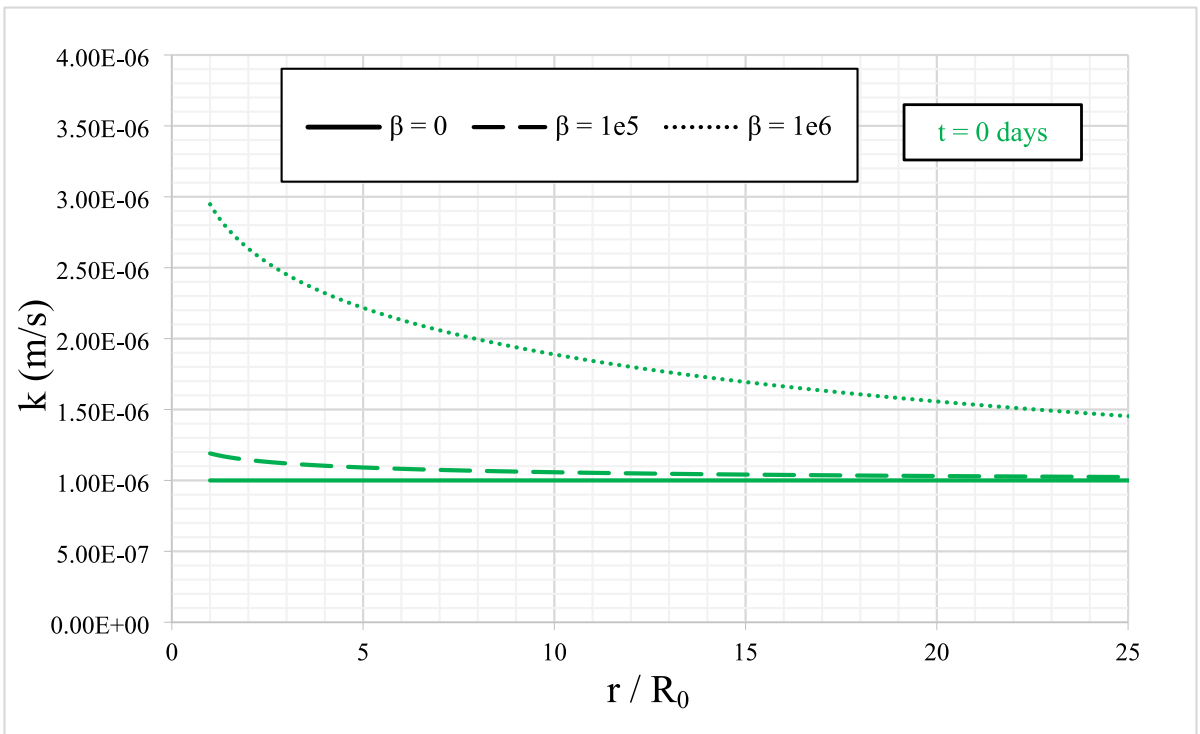
β = 0
β = 1e5
β = 1e6
t = 0 days
k (m/s)
4.00E-06
3.50E-06
3.00E-06
2.50E-06
2.00E-06
1.50E-06
1.00E-06
5.00E-07
0.00E+00
0
5
10
15
20
25
r / R0

◂**Fig. 8** Distributions of **a** displacements and **b** permeability coefficients when the rock mass behavior is governed by the Burgers model. Key: r: radial distance from the tunnel center, R_0: tunnel radius, k: permeability of the rock mass, u: displacement, β: strain-dependent permeability constant, t: time

- *Excavation of the tunnel:* The tunnel is excavated and the pore water pressure is set to zero at the tunnel boundary to simulate the drained condition;
  - *Running the model for $t=0$*: The hydraulic analysis is firstly carried out and the mechanical analysis is then performed. Therefore, a steady-state pore water pressure distribution is obtained in the hydraulic analysis, and this is then used as input data for the mechanical analysis. In the mechanical analysis, the water bulk modulus is set to zero to prevent extra pore water pressure being generated from mechanical deformations. This type of analysis is the so called "uncoupled method". As the coupled analysis (i.e., simultaneous hydraulic/mechanical analyses) is too time-consuming in the tridimensional numerical modelling, the uncoupled analysis was chosen. In Fig. 4a, the pore water distribution before the lining installation is shown.

Note that the time after which the steady state is reached can be estimated by

$$t_c^f = \frac{L_c^2}{Mk \times 10^{-4}} \tag{1}$$

where L_c is the average length of the flow path through the rock mass (unit: m), k is the rock mass permeability $\left(\text{unit} : \frac{\text{m}}{\text{s}}\right)$, and M is the Biot modulus (unit: Pa) which is equal to $\frac{K_w}{n}$. K_w is the water bulk modulus (unit: Pa) and n is the rock mass porosity (in this paper, the values of K_w and n are selected as 2 GPa and 0.5, respectively).

- The permeability of the rock mass is considered variable (see Fig. 5) as a function of the volumetric strain (ε_V) (Brown and Bray 1982) i.e.,

$$k = k_{ini}\left(1 + \beta\left(\varepsilon_V\right)^2\right) \tag{2}$$

where k_{ini} is the initial permeability of rock mass prior to the tunnel excavation, and β is the strain-dependent permeability constant. The value of β depends on the spacing of fractures, the number of rock mass fractures, and the fractures aperture (Brown and Bray 1982). By default, the permeability coefficient of the rock mass remains constant in FLAC^{3D} code. Thus, an algorithm able to vary the permeability coefficient in the model is implemented into the FLAC^{3D} software through a specific subroutine;

- *Analysis for $t>0$ till lining installation*: The previous step is conducted for $t=0$. But the current step is conducted for $t>0$. As the water flow is in the steady-state condition, it is not necessary to perform the hydraulic analysis again. Thus, it is necessary to perform only the creep analysis in the current step. In the creep analysis, the out-of-balance forces should be minimal; and therefore, it is recommended that the chosen time-step in the creep analysis become smaller than the maximum time-step (Δt_{max}^{cr}) (Itasca Consulting Group, 2020). Note that in Eq. 3, G_M is Maxwell shear modulus. η_M and η_K are Maxwell and Kelvin viscosities, respectively. Besides, G_K is the Kelvin shear modulus.

$$\Delta t_{max}^{cr} = \min\left(\frac{\eta_M}{G_M}, \frac{\eta_K}{G_K}\right) \tag{3}$$

  - *Lining installation*: An elastic lining with inner and outer radii of R_{in} and R_0 is installed at time t_1. It is assumed that the lining is porous. The assumption is based on practical observations and engineering realities. Indeed, even well-designed tunnel linings may exhibit some level of permeability due to micro cracks or cracks. As the lining is assumed to be porous, water can seep through it and consequently, the pore water pressure in the outer surface of the lining will be increased. But in the inner surface of the lining, the pore water pressure is set to zero to simulate the drained condition. Furthermore, the boundary nodes are restricted so that only radial displacements can occur;
  - *Running the model in new condition*: Before performing the mechanical analysis,

the velocities are set to zero because when switching from the creep analysis to the static analysis, the developed velocities are inappropriate for the static analysis (Itasca Consulting Group, 2020). Then, the hydro-mechanical analysis is performed for the time immediately after the lining installation. Afterword, the creep analyses are conducted till filling the tunnel with water. In Fig. 4b, the pore water distribution after the lining installation is depicted;

- • *Filling the tunnel with water:* At time t_2, the tunnel is filled with water to transport water from a reservoir to a powerhouse. The pore water pressure and total radial stress are set to the value of the internal water pressure at the inner radius of the lining;
  - *Running the model in final condition*: The velocities are again set to zero. Then, the hydro-mechanical analysis is performed for the time immediately after filling the tunnel with water. The creep analysis is then conducted for the necessary time. The pore water distribution after filling the tunnel with water is shown in Fig. 4c.

4 Results and Discussions

4.1 Verification

The accuracy of predictions by the numerical simulation can be verified by analytical solutions (Cardu et al. 2019; Oggeri et al. 2021). Figure 6 shows the short-term behavior obtained by using the procedures proposed by Bobet (2010) and by the numerical modelling (for the input data of Table 1); they show a very good agreement.

Recently, Zaheri et al. (2023b) proposed an analytical method to obtain the long-term response of deep submerged tunnels embedded in saturated rock masses. In this method, the behavior of the rock mass was considered viscoelastic obeying the Burgers model. Furthermore, the rock mass permeability coefficient was also considered variable as a function of the volumetric strain. In Fig. 7, the results of the numerical analysis are compared with those by this analytical method for the input values reported in Table 2. As seen, at $t = 1$ year, the internal water pressure is applied to the tunnel boundary. This causes the pore water pressure to increase at the outer radius of the lining. As this pressure is greater than the initial pore water pressure, water seeps toward the rock mass, and consequently, seepage forces decrease which leads displacements to diminish at $t = 1$ year. As times elapse, the tunnel convergences increase over time due to the rheological behavior of the saturated rock mass.

A satisfactory agreement between the results of numerical method with those by the analytical one implies the efficiency of the adopted algorithm implemented in FLAC^{3D} to consider a variable permeability coefficient. Therefore, the elasto-visco-plastic model is assigned for the rock mass in order to investigate the problem with a more realistic behavior.

4.2 Parametric Study

In the following subsections, the effect of:

- Variable permeability over time;
- The ratio of lining permeability to the rock mass permeability;
- The internal water pressure; and
- Rheological parameters

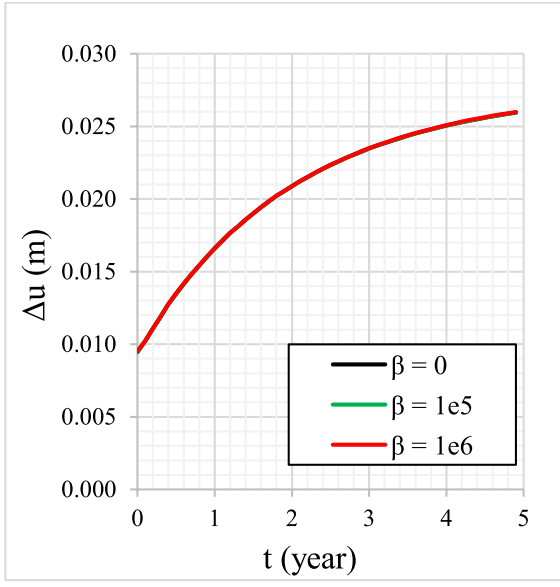

Fig. 9 Induced difference in the tunnel wall displacement (Δu) over time (t) when the rock mass behavior is governed by the Burgers model. Key: β: strain-dependent permeability constant

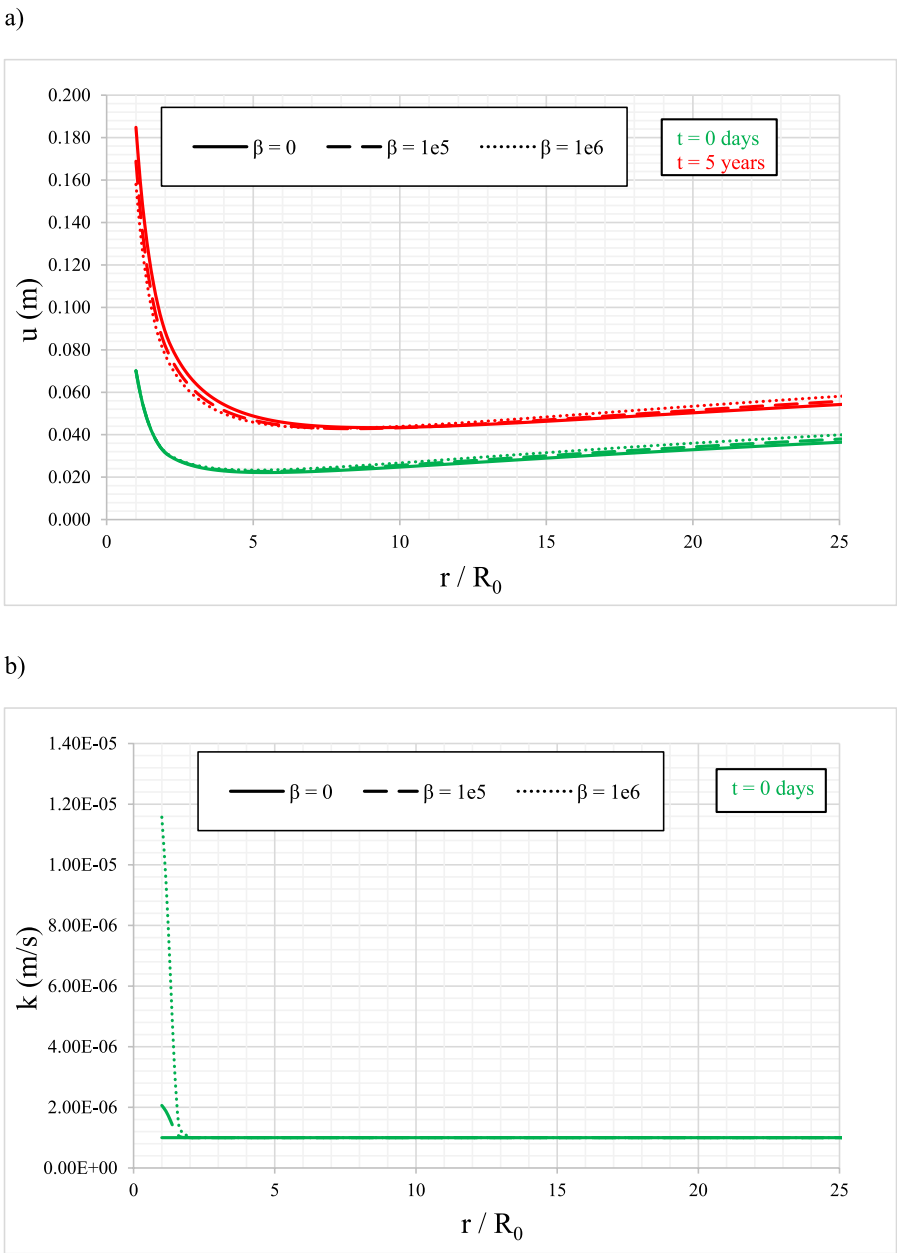

Fig. 10 Distributions of **a** displacements and **b** permeability coefficients when the rock mass behavior is governed by the CVISC model. Key: r: radial distance from the tunnel center, R_0: tunnel radius, k: permeability of the rock mass, u: displacement, β: strain-dependent permeability constant,t: time

are followed up on the submerged tunnel behavior with input data provided in Table 2.

4.2.1 Without Supporting System

4.2.1.1 The Influence of Variable Permeability of Rock Mass As stated, the permeability of the rock mass is considered variable as a function of the volumetric strain (ε_V) (Brown and Bray 1982) (see Eq. 2). The value of the β parameter (strain-dependent permeability constant) in this equation depends on the number of rock mass fractures, spacing of fractures, and their aperture.

As observed in Fig. 8, the greater the β parameter, the greater the rock mass displacement (u). In addition, the difference of displacements is intensified by moving away from the tunnel wall. Figure 9 shows the difference of the displacements over time (t) in

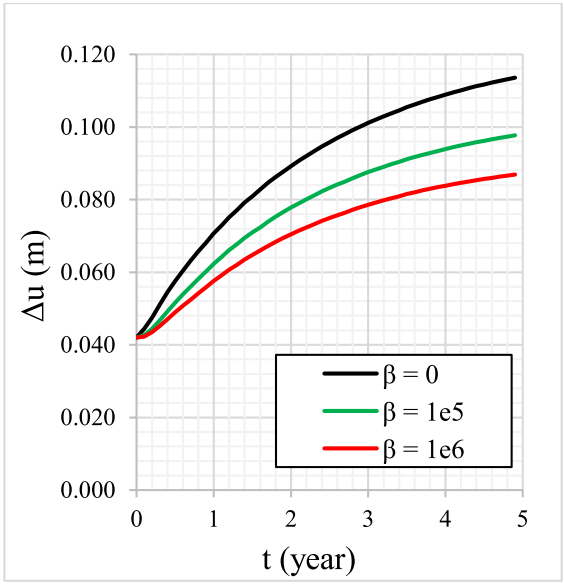

Fig. 11 Induced tunnel wall displacement (Δu) over time (t) when the rock mass behavior is governed by the CVISC model. Key: β: strain-dependent permeability constant

cases of with and without considering seepage influence, which indicates the tunnel wall displacement is not much influenced by variation of the β factor.

If the rock mass behavior is elasto-visco-plastic, the difference of displacements of the rock mass at far distances from the tunnel center becomes small, for different β parameters (Fig. 10). This is because the rock mass permeability is only changed when the rock mass becomes plastic. Thus, the pore water pressure is not much influenced by the β parameter. On the other hand, close to the tunnel boundary, the rock mass with a lower β value experiences greater displacements. As can be seen in Fig. 11, unlike the case in which the rock mass behavior is governed by the Burgers model, the difference of the tunnel wall displacements in cases $\beta = 0$and $\beta = 10^6$ increases with time. This can be due to the alteration of stresses in the rock mass with time, and therefore, the alteration of plastic strains.

As the tunnel wall experiences a greater displacement when considering the CVISC model for rock mass (See Figs. 8 and 10), the rock mass permeability coefficient (k) will be also greater with respect to the Burgers model. It causes the seepage force in the vicinity of the tunnel wall to decrease in the CVISC model.

On the other hand, for the viscoelastic behavior, the displacement in each point of the rock mass becomes greater by increasing the β value. However, for the CVISC model, the rock mass displacement is greatest when $\beta = 0$ (disregarding alteration of the permeability coefficient) near the tunnel boundary whereas it becomes reveres at far distances from the tunnel boundary (See Figs. 9 and 10). This is because, in the vicinity of the tunnel wall, in the rock mass with $\beta = 0$, the pore water pressure is greater, and thus the rock mass has smaller strength than the rock mass with $\beta = 10^6$ (See Fig. 10).

4.2.2 After Lining Installation and Applying the Internal Water Pressure

Here, it is assumed that the time of the lining installation and of applying the internal water pressure are at $t_1 = 4$ days and $t_2 = 365$ days, respectively. Note that t_1 is the lining installation time and varies according to project conditions such as construction methods and rock mass properties. As t_1 increases (i.e., the lining is installed after a longer period), the displacements of the tunnel wall increase due to the time-dependent (rheological) behavior of the rock mass. This extended time before lining installation allows more deformation in the rock mass, leading to greater tunnel convergence. In extreme cases, if the installation time is too long, the additional deformation could lead to tunnel instability or even collapse. Therefore, the time of lining installation is a critical parameter that should be considered in each project.

As seen in Figs. 12 and 13, when the lining is installed, water seeps into the porous lining; and hence, the pore water distribution is altered which causes the rock mass displacement to decrease. Then, the rock mass displacement starts to increase until the time of applying the internal water pressure, which its magnitude equals to 1.2 times of the initial pore water pressure, p_{w0}. It leads the water to seep from the tunnel towards the rock mass.

Thus, the pore water pressure distribution in the lining and rock mass differs from the time before internal water pressure is exerted; and consequently, the rock mass displacement decreases. For example,

a)

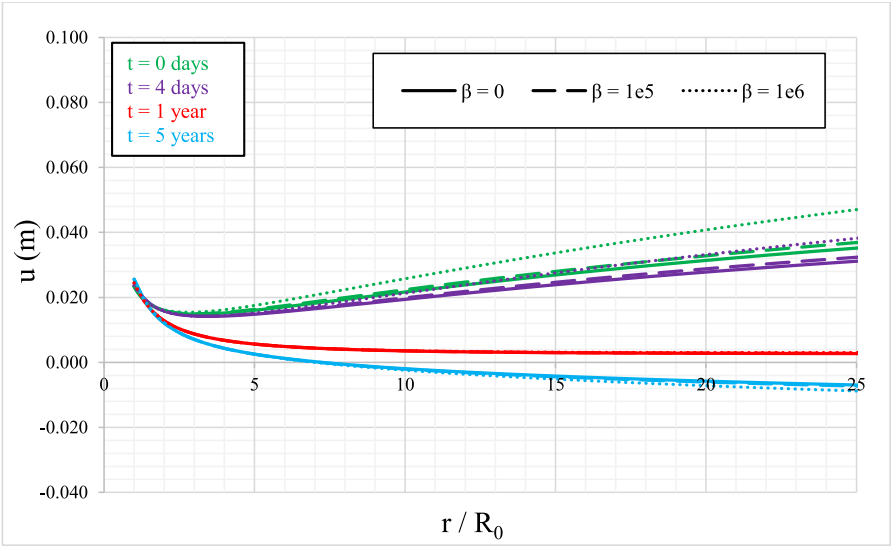

b)

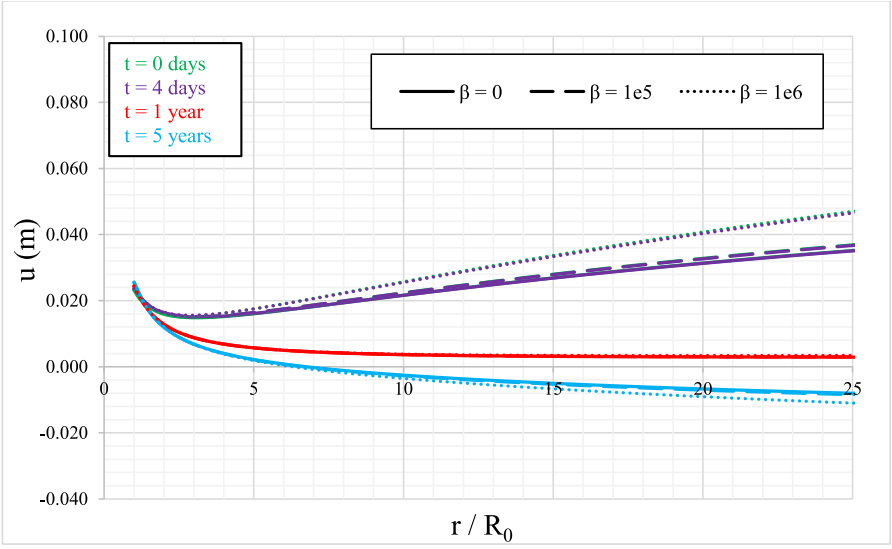

Fig. 12 Distribution of displacement when the rock mass behavior is governed by the Burgers model. **a** $\frac{k_{ini}}{k_{con}} = 10$, **b** $\frac{k_{ini}}{k_{con}} = 1$. Key: r: radial distance from the tunnel center, R_0: tunnel radius, k_{ini}: permeability of the rock mass, k_{con}: permeability of the lining, u: displacement, β: strain-dependent permeability constant, t: time

as Fig. 14 shows, when the rock mass behavior is governed by the Burgers model, the tunnel wall displacement decreases by about 14% after applying the internal water pressure. But for the CVISC model, this value is 5% (See Fig. 15). At far distances from the tunnel boundary, due to unloading from the rheological rock mass, rock mass displacements start to decrease gradually, for both viscoelastic and elasto-visco-plastic rock masses (Figs. 12 and 13).

On the other hand, the lining stress gradually enhances over time until the time of applying the internal water pressure (See Figs. 14 and 15). At t = 365 days, due to the increasing of the pore water pressure at the lining's outer radius, the total stress acting on the lining suddenly increases. For instance, for the Burgers and CVISC model, the total radial stress acting on the lining system increases of respectively 36% and 79%, after applying the internal water pressure.

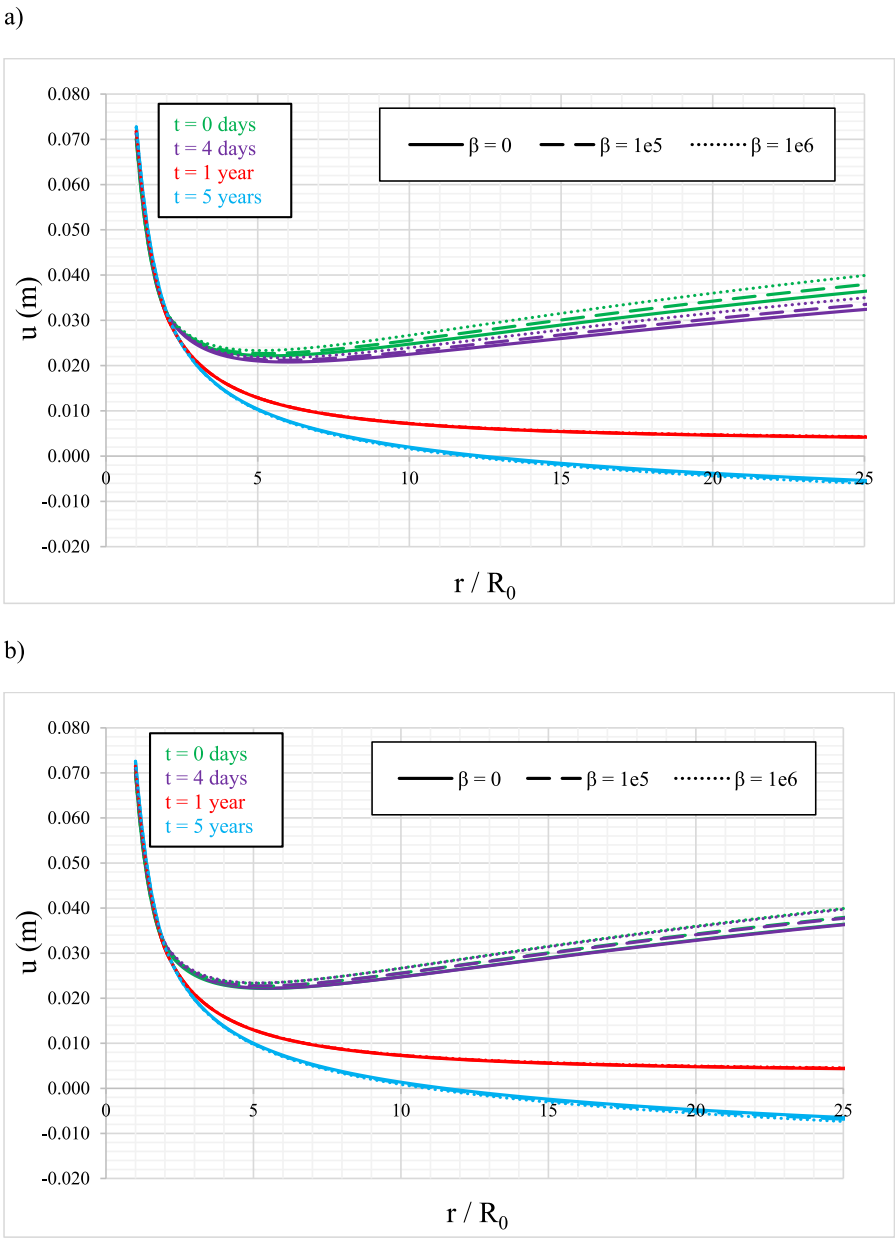

Fig. 13 Distribution of displacement when the rock mass behavior is governed by the CVISC model. **a** $\frac{k_{ini}}{k_{con}} = 10$, **b** $\frac{k_{ini}}{k_{con}} = 1$. Key: r: radial distance from the tunnel center, R_0: tunnel radius, k_{ini}: permeability of the rock mass, k_{con}: permeability of the lining, u: displacement, β: strain-dependent permeability constant, t: time

After that time, this stress gradually increases over time.

Unlike the tunnel wall convergence, the rock mass displacement is greatly influenced by the variation of β value in the viscoelastic rock mass (See Fig. 12). But in the elasto-visco-plastic rock mass, the variation of β does not show any influence on the rock mass behavior (See Fig. 13). On the other hand, after applying the internal water pressure, the rock mass displacements are negligibly influenced by the β factor.

4.2.2.1 The Influence of Ratio of the Rock Mass Permeability to the Lining Permeability The ratio of the rock mass permeability to the lining permeability is another parameter that can significantly affect the behavior of submerged tunnels. As Figs. 14 and 15 illustrate, before applying the internal water pressure and in the case $\frac{k_{ini}}{k_{con}} = 10$, there is almost a sig-

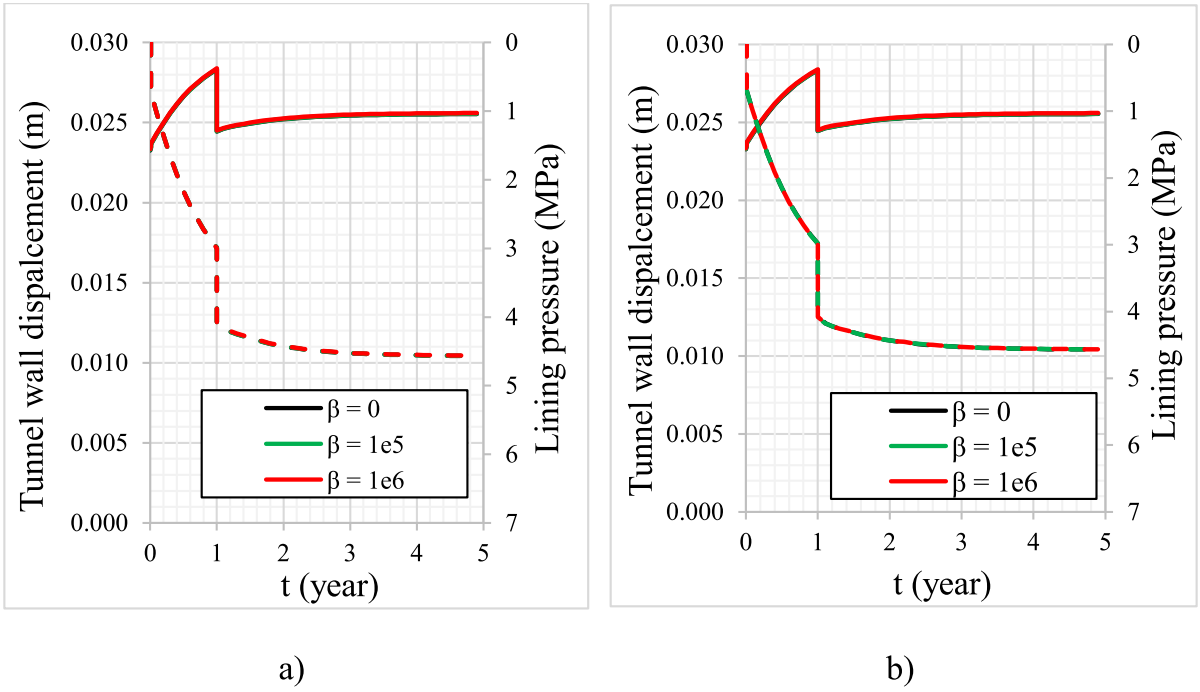

Fig. 14 Tunnel wall displacement (u) and total radial stress acting on the lining system (σ) over time (t). **a** $\frac{k_{ini}}{k_{con}} = 10$, **b** $\frac{k_{ini}}{k_{con}} = 1$ (Burgers model). Key: k_{ini}: permeability of the rock mass, k_{con}: permeability of the lining, β: strain-dependent permeability constant

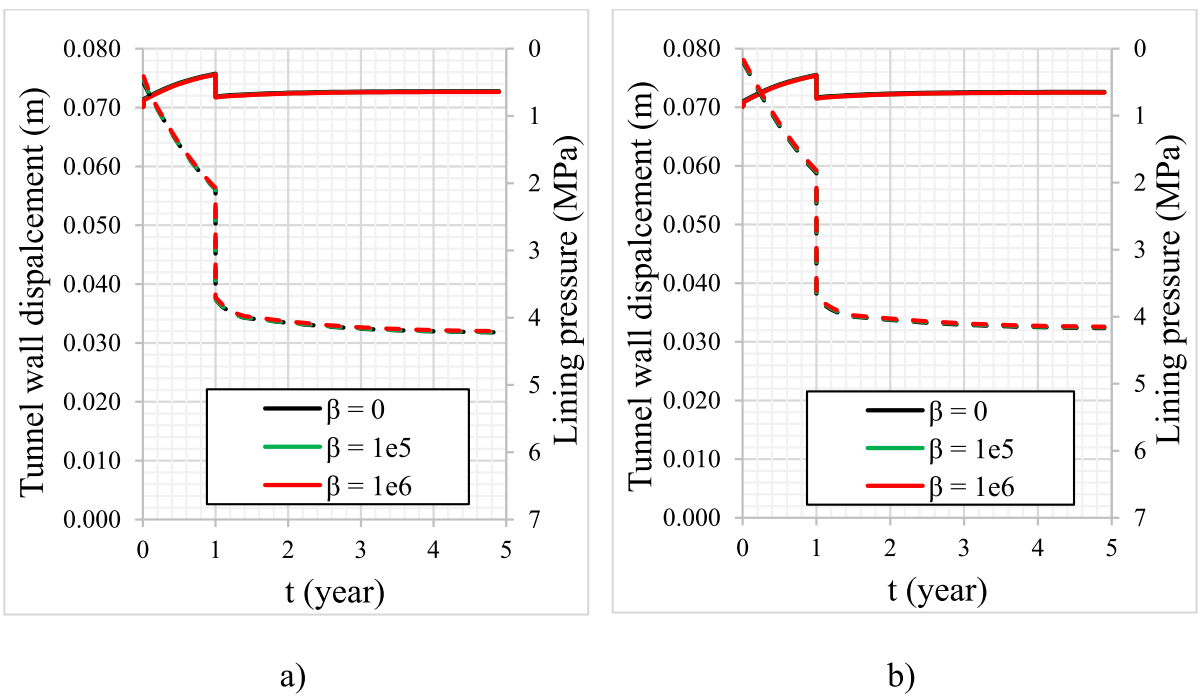

Fig. 15 Tunnel wall displacement (u) and total radial stress acting on the lining system (σ) over time (t). **a** $\frac{k_{ini}}{k_{con}} = 10$, **b** $\frac{k_{ini}}{k_{con}} = 1$ (CVISC model). Key: k_{ini}: permeability of the rock mass, k_{con}: permeability of the lining, β: strain-dependent permeability constant

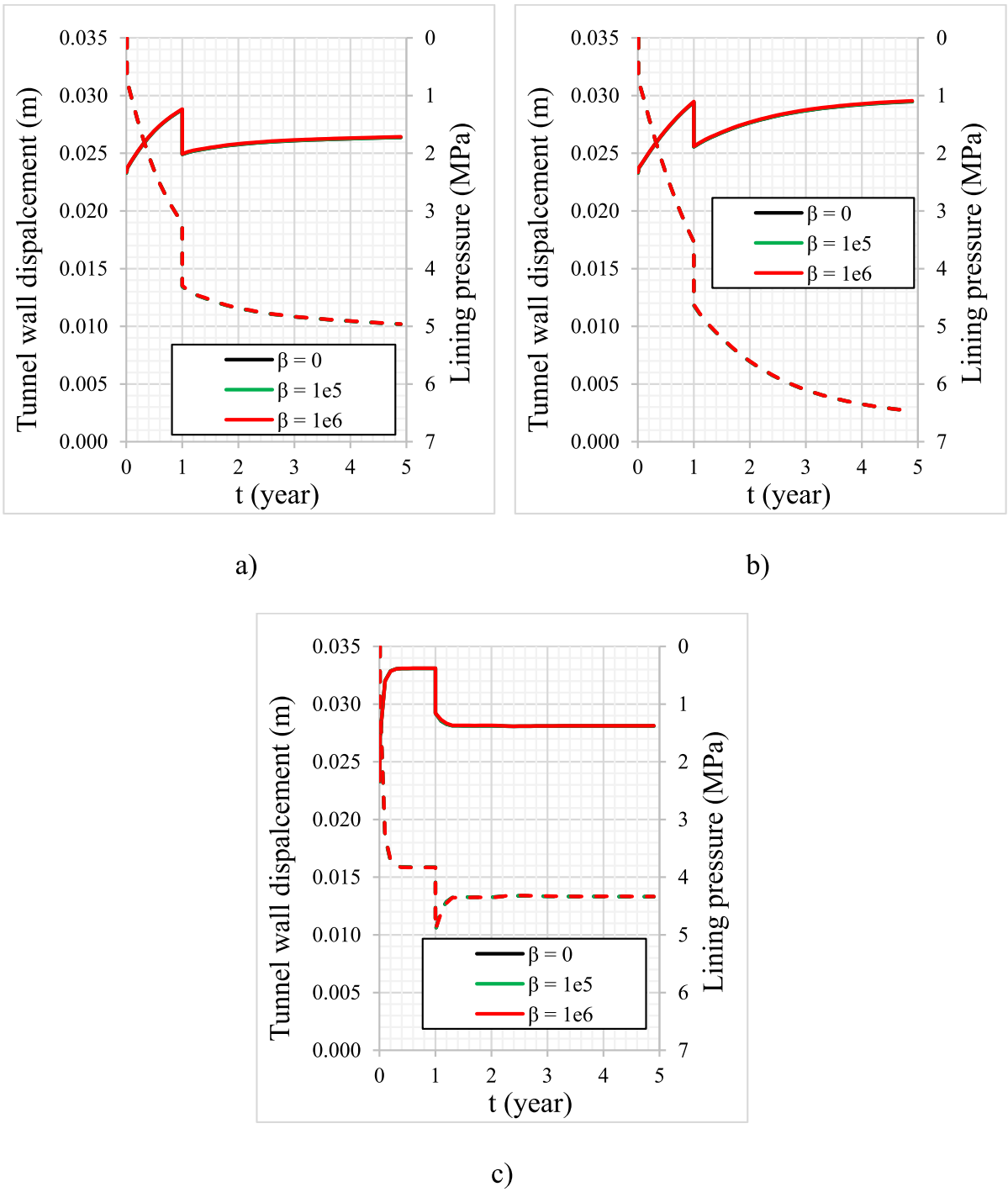

Fig. 16 Tunnel wall displacement (u) and total radial stress acting on the lining system (σ) over time (t). **a** $\eta_M = 0.05\ \eta_1$, $G_K = G_1$, $\eta_K = \eta_2$, **b** $\eta_M = \eta_1$,$G_K = 0.05\ G_1$, $\eta_K = \eta_2$, c) $\eta_M = \eta_1$, $G_K = G_1$, $\eta_K = 0.05\ \eta_2$ (Burgers model). Key: β: strain-dependent permeability constant

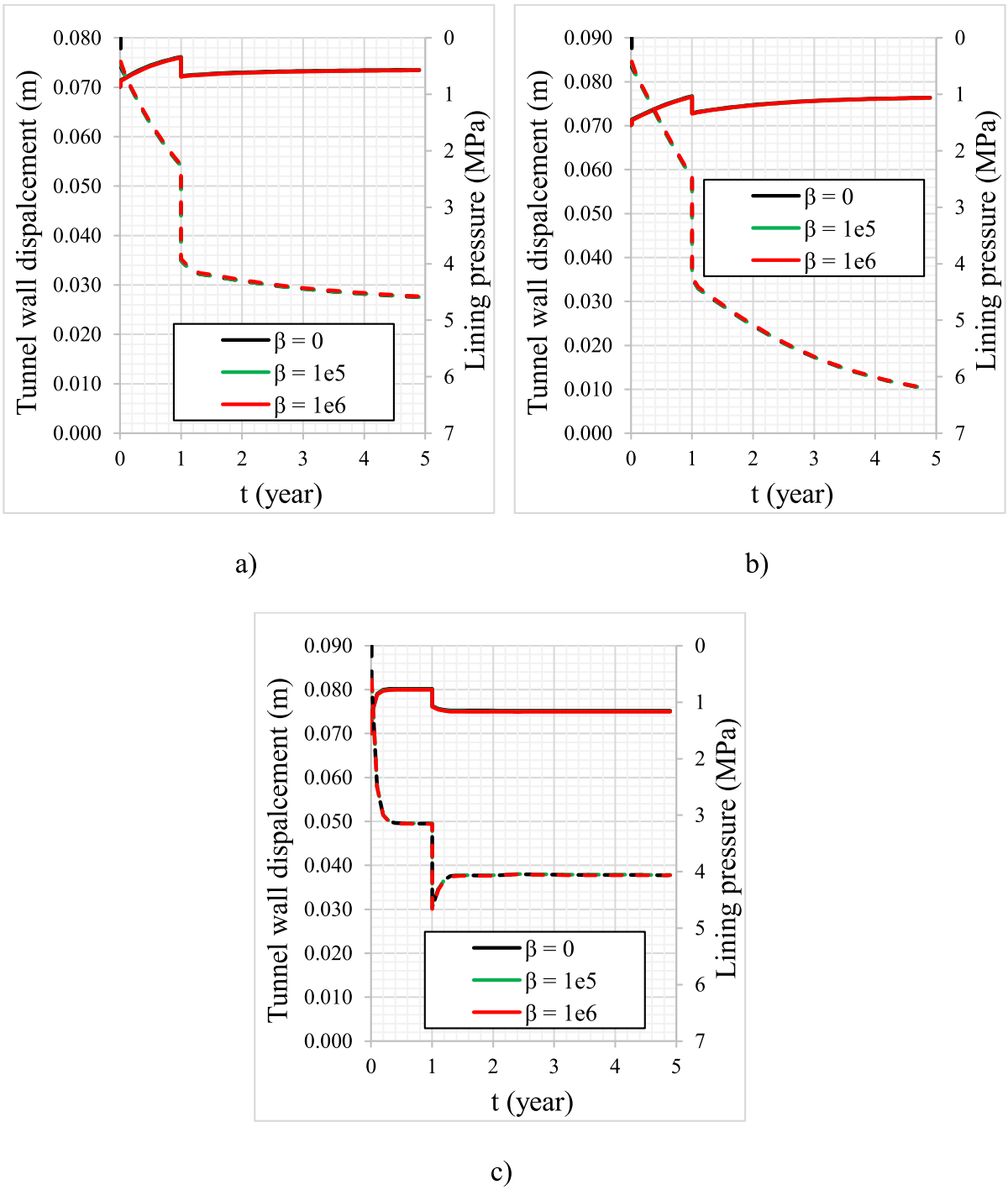

Fig. 17 Tunnel wall displacement (u) and total radial stress acting on the lining system (σ) over time (t). **a** $\eta_M = 0.05\ \eta_1$, $G_K = G_1$, $\eta_K = \eta_2$, **b** $\eta_M = \eta_1$,$G_K = 0.05\ G_1$, $\eta_K = \eta_2$, c) $\eta_M = \eta_1$, $G_K = G_1$, $\eta_K = 0.05\ \eta_2$ (CVISC model). Key: β: strain-dependent permeability constant

a)

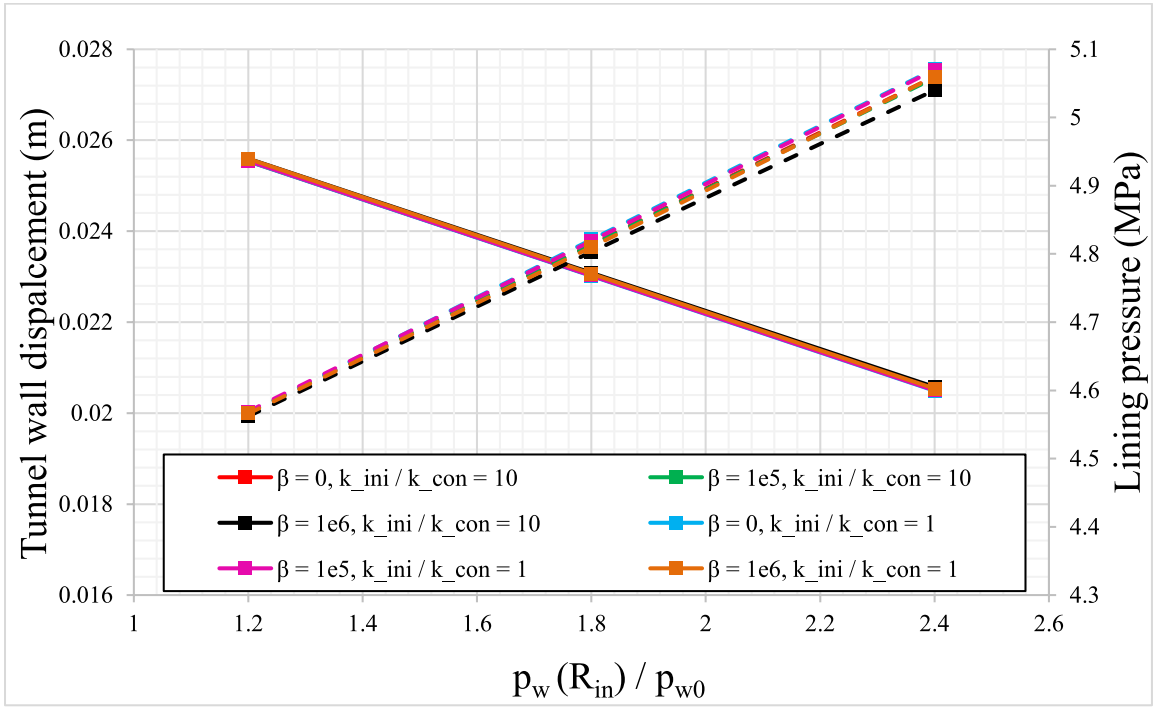
Tunnel wall dispalcement (m)
Lining pressure (MPa)
$p_w(R_{in}) / p_{w0}$
β = 0, k_ini / k_con = 10
β = 1e5, k_ini / k_con = 10
β = 1e6, k_ini / k_con = 10
β = 0, k_ini / k_con = 1
β = 1e5, k_ini / k_con = 1
β = 1e6, k_ini / k_con = 1

b)

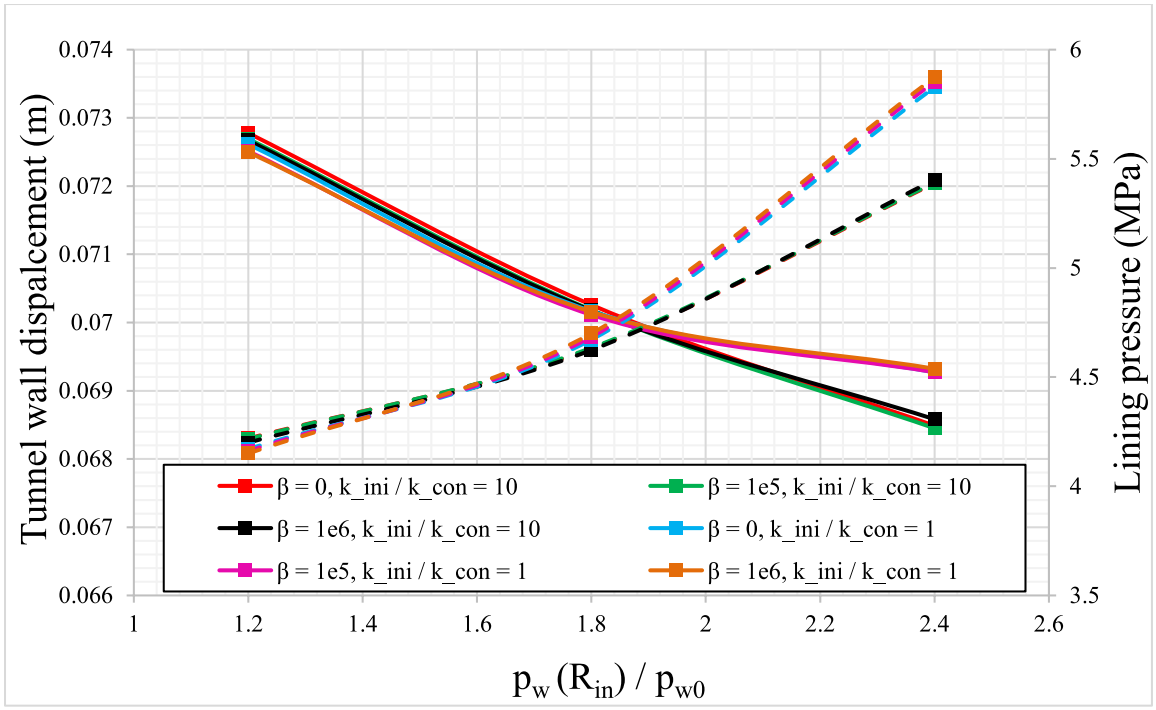
Tunnel wall dispalcement (m)
Lining pressure (MPa)
$p_w(R_{in}) / p_{w0}$
β = 0, k_ini / k_con = 10
β = 1e5, k_ini / k_con = 10
β = 1e6, k_ini / k_con = 10
β = 0, k_ini / k_con = 1
β = 1e5, k_ini / k_con = 1
β = 1e6, k_ini / k_con = 1

◂**Fig. 18** Tunnel wall displacement (u) and total radial stress acting on the lining system (σ) at $t = 5$ years. **a** Burgers model **b** CVISC model. Key: β: strain-dependent permeability constant, k_{ini}: permeability of the rock mass, k_{con}: permeability of the lining, $p_{w(R_{in})}$: pore water pressure at the inner radius of the lining, p_{w0}: initial pore water pressure

nificant difference between the rock mass and lining permeability coefficients, and when water seeps through the lining, a considerable loss of water pressure occurs. In this condition, a greater pore water pressure is exerted on the lining, and thus it can be expected that when $\frac{k_{ini}}{k_{con}} = 10$, the total lining pressure is higher than that in the case of $\frac{k_{ini}}{k_{con}} = 1$. Besides, when the rock mass behavior is governed by the CVISC model, as plastic zones appear around the tunnel, the deviatoric effective stress in the vicinity of the opening is lower than that in the rock mass with viscoelastic behavior. Thus, due to the lower deviatoric effective stress in the elasto-visco-plastic rock mass, it can be expected that the rock mass experiences lower displacements, and smaller pressure is exerted on the lining.

4.2.2.2 The Influence of the Rheological Parameters The effects of rheological parameters are investigated in this subsection. For this purpose, the values of the Maxwell viscosity, Kelvin shear modulus, and Kelvin viscosity are decreased by 95% from their initial values listed in Table 2. Note that η_1, G_1, and η_2 in Figs. 16 and 17 represent their initial values.

The comparison of Figs. 14 and 16 reveals, regardless of β value, when the values of $\eta_M = \eta_1$, $G_K = G_1$, and $\eta_K = \eta_2$ respectively are decreased to $0.05\eta_1$, $0.05G_1$, and $0.05\eta_2$, the tunnel convergence at $t = 1$ year (before applying the internal water pressure) increases about 1.7%, 3.9%, and 17% (at $t = 5$ years, these values change to 3.5%, 16%, and 10%, respectively). Therefore, the Kelvin shear modulus and Kelvin viscosity respectively have the greatest influence at $t = 1$ and 5 years. Note that when the value of η_K is selected as 0.05 times of η_2, the initial displacement rate is higher than the case with $\eta_K = \eta_2$.

After applying the internal water pressure, the tunnel wall displacement instantaneously decreases, due to the unloading condition. However, unlike the other cases, the tunnel convergences gradually decrease over time, and after elapsing some time, this condition is reversed.

On the other hand, when the rock mass behavior is governed by the CVISC model, as stated earlier, plastic zones appear around the tunnel, and therefore, the deviatoric effective stress in the vicinity of the tunnel is lower than that in the rock mass with viscoelastic behavior. Thus, due to the lower deviatoric effective stress in the elasto-visco-plastic rock mass, it can be expected that the percent increase in the tunnel wall displacements is smaller than that in the viscoelastic medium (See Figs. 15 and 17).

When the values of $\eta_M = \eta_1$, $G_K = G_1$, and $\eta_K = \eta_2$ respectively are decreased to $0.05\eta_1$, $0.05G_1$, and $0.05\eta_2$, the total stress acting on the lining at $t = 1$ year enhance about 7%, 18%, and 28% (at $t = 5$ years, these values will be 8%, 41%, and -5%, respectively). In the case $\eta_K = 0.05\eta_2$, due to the decrease of the tunnel wall displacement, this stress decreases gradually.

4.2.2.3 The Influence of the Internal Water Pressure The tunnel wall displacement (u) and the total radial stress acting on the lining system (σ) at $t = 5$ years in terms of $\frac{k_{ini}}{k_{con}}$, $\frac{p_{w(R_{in})}}{p_{w0}}$, and β values have been shown in Fig. 18. In the viscoelastic rock mass, by increasing the β value, the total radial stress acting on the lining system decreases; and consequently, the tunnel wall displacement increases (Fig. 18a). However, when the $\frac{k_{ini}}{k_{con}}$ ratio becomes greater, the rock mass experiences greater convergences (with lower σ). This is because, the seepage force is lower than the case with a lower $\frac{k_{ini}}{k_{con}}$ ratio, as stated previously.

Furthermore, $\frac{p_{w(R_{in})}}{p_{w0}}$ has the most notable influence on the tunnel response among the others. In a submerged tunnel with higher internal water pressure, the water pressure at the outer radius of the lining is greater and it leads the magnitude of the σ parameter to enhance (see Fig. 18).

However, as seen in Fig. 18b, for the CVISC model, the magnitudes of both u and σ are not altered linearly with $\frac{p_{w(R_{in})}}{p_{w0}}$, because the size of the plastic zone radius and plastic strains will be different when $\frac{p_{w(R_{in})}}{p_{w0}}$ ratio is altered.

Similar to the viscoelastic model, for greater $\frac{p_{w(R_{in})}}{p_{w0}}$ values, higher total radial stress values are exerted on the lining. On the contrary, investigation of $\frac{k_{ini}}{k_{con}}$ and β roles on the tunnel response reveals that their effects on the u and σ do not follow a unique trend; and the responses differ from case to case (see Fig. 18).

5 Conclusions

In this paper, the interaction of submerged tunnels and rock masses was investigated in detail, considering the construction phases of the tunnel. For this purpose, the simultaneous influence of the water seepage and the time-dependent behavior of the rock mass was considered. To simulate the rheological behavior of the rock mass, both the elasto-visco-plastic model (so called CVISC model) and Burgers viscoelastic model were assigned to the rock mass. In addition, the permeability coefficient of each point of the medium was assumed to vary with the volumetric strain, unlike the default assumption in geotechnical software packages in which this parameter is generally assumed constant throughout the analysis. The following distinguished conclusions are made:

- In the viscoelastic rock mass, by increasing the strain-dependent permeability constant (β), the difference of displacements becomes gradually more as distance from the tunnel wall increases;
- Unlike the viscoelastic rock mass in which the unsupported tunnel wall displacement is not influenced by considering variable permeability, in the case of visco plastic model, a difference in displacements exists when considering and disregarding the variable permeability, and this difference increases over time;
- After applying the internal water pressure, in the case of the viscoelastic model, the increasing the strain-dependent permeability constant value causes the total radial stress acting on the lining system to decrease;
- After applying the internal water pressure, the increase of the ratio of lining permeability to the rock mass permeability leads the rock mass to have greater convergences but to exert a lower total radial stress on the lining;
- The magnitudes of both the tunnel wall displacement and the total stress acting on the lining are not altered linearly by increasing the value of the internal water pressure.

From a practical perspective, accounting for time-dependent permeability in rock masses with time-dependent behaviour makes the problem more complex, as it requires considering hydro-mechanical interactions. Despite this, the results show that including the variability of permeability coefficients improves the accuracy of tunnel displacement predictions. Therefore, incorporating time-dependent permeability into geotechnical software is both feasible and highly beneficial for practical use.

Author Contributions Milad Zaheri: Conceptualization, methodology, writing—original; Masoud Ranjbarnia: Conceptualization, methodology, writing—review; Pierpaolo Oreste: Conceptualization, methodology, writing—review.

Funding Open access funding provided by Politecnico di Torino within the CRUI-CARE Agreement. The authors have not disclosed any funding.

Data Availability No data was used for the research described in the article.

Declarations

Conflict of interest We declare that we have no financial and personal relationships with other people or organizations that can inappropriately influence our work, there is no professional or other personal interest of any nature or kind in any product, service and/or company that could be construed as influencing the position presented in, or the review of, the manuscript entitled.

References

Ai ZY, Pan YX, Ye ZK, Wang DS (2025) Fractional viscoelastic analysis of transversely isotropic surrounding rock along shallow buried elliptical tunnel. Int J Numer Anal Meth Geomech 49(1):329–344

Bobet A (2001) Analytical solutions for shallow tunnels in saturated ground. J Eng Mech 127(12):1258–1266. https://doi.org/10.1061/(ASCE)0733-9399(2001)127:12(1258)

Bobet A (2010) Characteristic curves for deep circular tunnels in poroplastic rock. Rock Mech Rock Eng 43(2):185–200. https://doi.org/10.1007/s00603-009-0063

Bobet A, Nam SW (2007) Stresses around pressure tunnels with semi-permeable liners. Rock Mech Rock Eng 40(3):287–315. https://doi.org/10.1007/s00603-006-0123-6

Brown E, Bray J (1982) Rock-support interaction calculations for pressure shafts and tunnels. Paper presented at the ISRM international symposium.

Cardu M, Coragliotto D, Oreste P (2019) Analysis of predictor equations for determining the blast-induced vibration in rock blasting. Int J Min Sci Technol 29(6):905–915

Carranza-Torres C, Zhao J (2009) Analytical and numerical study of the effect of water pressure on the mechanical response of cylindrical lined tunnels in elastic and elastoplastic porous media. Int J Rock Mech Min Sci 46(3):531–547. https://doi.org/10.1016/j.ijrmms.2008.09.009

Chen X, He C, Xu G, Wang B, Ma G, Du J (2025) Stabilisation time analysis method for deep tunnels considering rheological effects and lining influence. Tunn Undergr Space Technol 155:106170

Chu Z, Wu Z, Liu B, Liu Q (2019) Coupled analytical solutions for deep-buried circular lined tunnels considering tunnel face advancement and soft rock rheology effects. Tunn Undergr Space Technol 94:103111. https://doi.org/10.1016/j.tust.2019.103111

Chu Z, Wu Z, Liu Q, Liu B (2020) Analytical solutions for deep-buried lined tunnels considering longitudinal discontinuous excavation in rheological rock mass. J Eng Mech 146(6):04020047. https://doi.org/10.1061/(ASCE)EM.1943-7889.0001784

Chu Z, Wu Z, Liu Q, Liu B, Sun J (2021) Analytical solution for lined circular tunnels in deep viscoelastic burgers rock considering the longitudinal discontinuous excavation and sequential installation of liners. J Eng Mech 147(4):04021009. https://doi.org/10.1061/(ASCE)EM.1943-7889.0001912

Dadashi E, Noorzad A, Shahriar K, Goshtasbi K (2017) Hydromechanical interaction analysis of reinforced concrete lining in pressure tunnels. Tunn Undergr Space Technol 69:125–132. https://doi.org/10.1016/j.tust.2017.06.006

de Rienzo F, Oreste P, Pelizza S (2009) 3D GIS supporting underground urbanisation in the City of Turin (Italy). Geotech Geol Eng 27(4):539–547

Do N-A, Dias D, Oreste P, Djeran-Maigre I (2015) Behaviour of segmental tunnel linings under seismic loads studied with the hyperstatic reaction method. Soil Dyn Earthq Eng 79:108–117

Do D-P, Tran N-T, Mai V-T, Hoxha D, Vu M-N (2020) Time-dependent reliability analysis of deep tunnel in the viscoelastic burger rock with sequential installation of liners. Rock Mech Rock Eng 53(3):1259–1285. https://doi.org/10.1007/s00603-019-01975-6

Do D-P, Vu M-N, Tran N-T, Armand G (2021) Closed-form solution and reliability analysis of deep tunnel supported by a concrete liner and a covered compressible layer within the viscoelastic burger rock. Rock Mech Rock Eng 54(5):2311–2334. https://doi.org/10.1007/s00603-021-02401-6

Fahimifar A, Zareifard MR (2014) A new elasto-plastic solution for analysis of underwater tunnels considering strain-dependent permeability. Struct Infrastruct Eng 10(11):1432–1450. https://doi.org/10.1080/15732479.2013.824489

Fahimifar A, Tehrani FM, Hedayat A, Vakilzadeh A (2010) Analytical solution for the excavation of circular tunnels in a visco-elastic Burger's material under hydrostatic stress field. Tunn Undergr Space Technol 25(4):297–304. https://doi.org/10.1016/j.tust.2010.01.002

Fahimifar A, Ghadami H, Ahmadvand M (2014) The influence of seepage and gravitational loads on elastoplastic solution of circular tunnels. Sci Iran Trans A Civ Eng 21(6):1821

Fahimifar A, Ghadami H, Ahmadvand M (2015a) An elasto-plastic model for underwater tunnels considering seepage body forces and strain-softening behaviour. Eur J Environ Civ Eng 19(2):129–151. https://doi.org/10.1080/19648189.2014.939305

Fahimifar A, Ghadami H, Ahmadvand M (2015b) The ground response curve of underwater tunnels, excavated in a strain-softening rock mass. Geomech Eng 8(3):323–359. https://doi.org/10.12989/gae.2015.8.3.323

Guo Z, Wu B, Jia S (2021) An analytical model for predicting the mechanical behavior of a deep lined circular pressure tunnel by using complex variable method. Geomech Geophys Geo-Energy Geo-Resour 7(4):90. https://doi.org/10.1007/s40948-021-00282-1

Hongming T, Zheyuan Z, Weizhong C, Xianjun T, Dong W, Jianxian Y (2024) Effects of the compressible layer on the long-term stability of secondary lining in a squeezing tunnel. Tunn Undergr Space Technol 149:105787

Hu X, Gutierrez M (2023) Viscoelastic Burger's model for tunnels supported with tangentially yielding liner. J Rock Mech Geotech Eng 15(4):826–837. https://doi.org/10.1016/j.jrmge.2022.07.013

Itasca Consulting Group I (2020) FLAC3D Version 7.0, Fast lagrangian analyses of continua in three-dimensions

Jing W, Zhou J, Yuan L, Jin R, Jing L (2023) Deformation and failure mechanism of surrounding rock in deep soft rock tunnels considering rock rheology and different strength criteria. Rock Mech Rock Eng. https://doi.org/10.1007/s00603-023-03565-z

Kanji M, He M, Ribeiro L, eSousa (2019) Soft rock mechanics and engineering. Springer, Cham. https://doi.org/10.1007/978-3-030-29477-9

Kargar AR (2019) An analytical solution for circular tunnels excavated in rock masses exhibiting viscous elastic-plastic behavior. Int J Rock Mech Min Sci 124:104128. https://doi.org/10.1016/j.ijrmms.2019.104128

Kargar AR, Haghgouei H (2020) An analytical solution for time-dependent stress field of lined circular tunnels using complex potential functions in a stepwise procedure. Appl Math Model 77:1625–1642. https://doi.org/10.1016/j.apm.2019.09.025

Kargar AR, Haghgouei H, Babanouri N (2020) Time-dependent analysis of stress components around lined tunnels with circular configuration considering tunnel advancing rate effects. Int J Rock Mech Min Sci 133:104422. https://doi.org/10.1016/j.ijrmms.2020.104422

Kolymbas D, Wagner P (2007) Groundwater ingress to tunnels–the exact analytical solution. Tunn Undergr Space Technol 22(1):23–27. https://doi.org/10.1016/j.tust.2006.02.001

Li C, Zaheri M, Ranjbarnia M, Daniel DIAS (2023) Calculating of the tunnel face deformations reinforced by longitudinal fiberglass dowels: from analytical method to artificial intelligence. Transp Geotech 43:101152. https://doi.org/10.1016/j.trgeo.2023.101152

Liang Y, Zha W, Shuai Y, Xu T (2025) Predicting optimal support timing for secondary tunnel lining based on creep damage in rock-support systems. Geotech Geol Eng 43(1):45

Liu C, Zhang D, Zhang S, Fang Q, Sun Z (2023) Long-term mechanical analysis of tunnel structures in rheological rock considering the degradation of primary lining. Undergr Space 10:217–232. https://doi.org/10.1016/j.undsp.2022.10.005

Lu W, Song S, Li S, Liang B, Li J, Luan Y, Wang L, Sun H (2024) Study on mechanical properties of composite support structures in TBM tunnel under squeezing soft rock conditions. Tunn Undergr Space Technol 144:105530

Nomikos P, Rahmannejad R, Sofianos A (2011) Supported axisymmetric tunnels within linear viscoelastic burgers rocks. Rock Mech Rock Eng 44(5):553–564. https://doi.org/10.1007/s00603-011-0159-0

Oggeri C, Oreste P, Spagnoli G (2021) The influence of the two-component grout on the behaviour of a segmental lining in tunnelling. Tunn Undergr Space Technol 109:103750

Oreste P (2009) Face stabilisation of shallow tunnels using fibreglass dowels. Proc Inst Civ Eng Geotech Eng 162(2):95–109

Paraskevopoulou C, Diederichs M (2018) Analysis of time-dependent deformation in tunnels using the convergence-confinement method. Tunn Undergr Space Technol 71:62–80. https://doi.org/10.1016/j.tust.2017.07.001

Pelizza S, Oreste P, Peila D, Oggeri C (2000) Stability analysis of a large cavern in Italy for quarrying exploitation of a pink marble. Tunn Undergr Space Technol 15(4):421–435

Ranjbarnia M, Fahimifar A, Oreste P (2014) A simplified model to study the behavior of pre-tensioned fully grouted bolts around tunnels and to analyze the more important influencing parameters. J Min Sci 50(3):533–548

Rocscience I (2007) RocLab Version 1.031—Rock mass strength analysis using the Hoek–Brown failure criterion. In.

Song F, Rodriguez-Dono A, Sanchez Farfan P (2022) Modelling underground excavations in rock masses with anisotropic time-dependent behaviour. Geomech Geophys Geo-Energy Geo-Resour 8(5):146. https://doi.org/10.1007/s40948-022-00440-z

Tarifard A, Görög P, Török Á (2022) Long-term assessment of creep and water effects on tunnel lining loads in weak rocks using displacement-based direct back analysis: an example from northwest of Iran. Geomech Geophys Geo-Energy Geo-Resour 8(1):31. https://doi.org/10.1007/s40948-022-00342-0

Tran Manh H, Sulem J, Subrin D, Billaux D (2015) Anisotropic time-dependent modeling of tunnel excavation in squeezing ground. Rock Mech Rock Eng 48(6):2301–2317. https://doi.org/10.1007/s00603-015-0717-y

Wang HN, Li Y, Ni Q, Utili S, Jiang MJ, Liu F (2013) Analytical solutions for the construction of deeply buried circular tunnels with two liners in rheological rock. Rock Mech Rock Eng 46(6):1481–1498. https://doi.org/10.1007/s00603-012-0362-7

Wang H, Jiang M, Zhao T, Zeng G (2019) Viscoelastic solutions for stresses and displacements around non-circular tunnels sequentially excavated at great depths. Acta Geotech 14(1):111–139. https://doi.org/10.1007/s11440-018-0634-9

Wang H, Song F, Zhao T, Jiang M (2020) Solutions for lined circular tunnels sequentially constructed in rheological rock subjected to non-hydrostatic initial stresses. Eur J Environ Civ Eng. https://doi.org/10.1080/19648189.2020.1737576

Wang G, Fang W, Han W, Jiang Y, Zhang X, Xu F, Zhang S (2023) Coupled rheological behavior of tunnel rock masses reinforced by rock bolts based on the non-hydrostatic stress field. Tunn Undergr Space Technol 137:105123

Wu K, Shao Z (2019a) Study on the effect of flexible layer on support structures of tunnel excavated in viscoelastic rocks. J Eng Mech 145(10):04019077. https://doi.org/10.1061/(ASCE)EM.1943-7889.0001657

Wu K, Shao Z (2019b) Visco-elastic analysis on the effect of flexible layer on mechanical behavior of tunnels. Int J Appl Mech 11(03):1950027. https://doi.org/10.1142/S1758825119500273

Wu K, Shao Z, Qin S, Zhao N (2019) Mechanical analysis of tunnels supported by yieldable steel ribs in rheological rocks. Geomech Eng 19(1):61–70. https://doi.org/10.12989/gae.2019.19.1.061

Wu K, Shao Z, Qin S (2020a) An analytical design method for ductile support structures in squeezing tunnels. Arch Civ Mech Eng 20(3):91. https://doi.org/10.1007/s43452-020-00096-0

Wu K, Shao Z, Hong S, Qin S (2020b) Analytical solutions for mechanical response of circular tunnels with double primary linings in squeezing grounds. Geomech Eng 22(6):509–518

Wu K, Shao Z, Li C, Qin S (2020c) Theoretical investigation to the effect of bolt reinforcement on tunnel viscoelastic behavior. Arab J Sci Eng 45(5):3707–3718. https://doi.org/10.1007/s13369-019-04215-9

Wu K, Shao Z, Qin S, Zhao N, Hu H (2020d) Analytical-based assessment of effect of highly deformable elements on tunnel lining within viscoelastic rocks. Int J Appl Mech 12(03):2050030. https://doi.org/10.1142/S1758825120500301

Zaheri M, Ranjbarnia M (2021) Ground reaction curve of a circular tunnel considering the effects of the altered zone and the self-weight of the plastic zones. Eur J Environ Civ Eng 26(11):4973–4997. https://doi.org/10.1080/19648189.2021.1877829

Zaheri M, Ranjbarnia M (2023a) Long-term analysis of tunnels in rheological rock masses considering the excavation-damaged zone. Int J Geomech 23(1):04022266. https://doi.org/10.1061/(ASCE)GM.1943-5622.0002642

Zaheri M, Ranjbarnia M (2023b) Theoretical and numerical analyses of squeezing rock mass around a spherical opening considering the existence of a damaged zone. Amirkabir J Civ Eng. https://doi.org/10.22060/CEEJ.2022.20529.7452

Zaheri M, Ranjbarnia M (2024) An analytical–numerical method for the hydraulic–mechanical coupling analysis of time-dependent behavior of pressurized tunnels: impact of an excavation damaged zone. Comput Geotech 170:106299. https://doi.org/10.1016/j.compgeo.2024.106299

Zaheri M, Ranjbarnia M, Goudarzy M (2022) Analytical and numerical simulations to predict the long-term behavior of lined tunnels considering excavation-induced damaged zone. Rock Mech Rock Eng. https://doi.org/10.1007/s00603-022-02962-0

Zaheri M, Ranjbarnia M, Dias D (2023a) New analytical approach to simulate the longitudinal fiberglass dowels performance installed at the face of a tunnel embedded in weak and weathered rock masses. Comput Geotech 153:105080. https://doi.org/10.1016/j.compgeo.2022.105080

Zaheri M, Ranjbarnia M, Zareifard MR (2023b) A theoretical solution to investigate long-term behavior of pressurized tunnels in severe squeezing conditions. Comput Geotech 159:105499. https://doi.org/10.1016/j.compgeo.2023.105499

Zaheri M, Li C, Ranjbarnia M, Dias D (2024a) Predicting long-term displacements of deep tunnels using an artificial neural network optimized by sand cat swarm optimization with Chebyshev map. Environ Earth Sci 83(8):228. https://doi.org/10.1007/s12665-024-11539-9

Zaheri M, Ranjbarnia M, Oreste P (2024b) Reliability analysis of deep pressurized tunnels excavated in the rock mass with rheological behavior. Transp Geotech 45:101212. https://doi.org/10.1016/j.trgeo.2024.101212

Zaheri M, Ranjbarnia M, Goudarzy M (2025) Time-dependent tunnel response: analytical & numerical solutions for non-linear post-peak behavior. Geotech Geol Eng 43(2):76. https://doi.org/10.1007/s10706-024-02968-1

Zareifard MR, Fahimifar A (2016a) Analytical solutions for the stresses and deformations of deep tunnels in an elastic-brittle-plastic rock mass considering the damaged zone. Tunn Undergr Space Technol 58:186–196. https://doi.org/10.1016/j.tust.2016.05.007

Zareifard MR, Fahimifar A (2016b) A simplified solution for stresses around lined pressure tunnels considering non-radial symmetrical seepage flow. KSCE J Civ Eng 20(7):2640–2654. https://doi.org/10.1007/s12205-016-0105-5

Zareifard MR, Shekari MR (2021) Comprehensive solutions for underwater tunnels in rock masses with different GSI values considering blast-induced damage zone and seepage forces. Appl Math Model 96:236–268. https://doi.org/10.1016/j.apm.2021.03.003

Zeng GS, Wang HN, Jiang MJ, Luo LS (2020) Analytical solution of displacement and stress induced by the sequential excavation of noncircular tunnels in viscoelastic rock. Int J Rock Mech Min Sci 134:104429. https://doi.org/10.1016/j.ijrmms.2020.104429

Zeng GS, Wang HN, Song F, Rodriguez-Dono A (2024) Time-dependent analytical solutions for tunnels excavated in anisotropic rheological rock masses. Tunn Undergr Space Technol 152:105890

Zhang Z, Liu X, Cheng L, Wu S, Zhang B (2020) A rheological constitutive model for damaged zone evolution of a tunnel considering strain hardening and softening. Geomech Geophys Geo-Energy Geo-Resour 6:1–17. https://doi.org/10.1007/s40948-020-00181-x

Zhao N, Shao Z, Chen X, Yuan B, Wu K (2022) Prediction of mechanical response of “a flexible support system” supported tunnel in viscoelastic geomaterials. Arch Civ Mech Eng 22(4):160. https://doi.org/10.1007/s43452-022-00485-7

Zhou J, Yang XA, Ma MJ, Li LH (2021) The support load analysis of deep-buried composite lining tunnel in rheological rock mass. Comput Geotech 130:103934. https://doi.org/10.1016/j.compgeo.2020.103934